Received: May 3, 2023. Revised: July 5, 2023.

INASS

International Journal of
Intelligent Engineering & Systems

http://www.inass.org/

An Optimized Uncertainty Aware Fine-Tuned Transfer Learning for COVID-19 Diagnosis from Medical Images

Deepika Selvam[1]* **Rajeswari Murugesan[1]**

[1]*Department of Computer science, PSGR Krishnanmal College for Women Coimbatore, Tamilnadu, India*
Corresponding author's Email: deepikasriselvam@gmail.com,

Abstract: In worldwide, COVID-19 has had a significant influence on patients and healthcare systems. Earlier stage of COVID-19 diagnosis and identification are the primary problems in the current pandemic condition. The identification of COVID-19 in CT and chest-X-ray (CXR) imaging is essential for diagnosis, treatment, and evaluation. However, radiologists face a foreseeable issue when it comes to coping with analytical ambiguity in medical imaging. In that situation, a paradigm based on convolutional neural network (CNN) with transfer learning (TL) and taking uncertainty into account was suggested to identify COVID-19 from CT and CXR scan images. However, this method was less capable to extract more useful and distinct image attributes. By fine-tuning the TL network design, this issue can be resolved. The fine tuning model can only fine tune specific layers associated with various goal objectives. However, one of the primary issues with such a method is the selection of layers. To solve this issue, this research uses an enhanced spider monkey optimization (ESMO) technique to select layers of ResNet architecture. Every population of an initialized spider monkey (SM) selects layer and parameter for fine tuning architecture. The fitness value of each SM is used to find best optimal solutions. Categorical cross-entropy loss (CCEL) is considered as fitness of SM. The fitness value of each SM is employed to determine the highest optimal solutions. Subsequent processes such as the stance update process, the learning and decision phase for the local and global leaders of ESMO algorithms, iteratively search for near optimal solutions until convergence. The proposed method can automatically estimate the various CNN layers, which can then be fine-tuned to extract more significant and discriminative features for efficient COVID-19 identification. Finally, the results reveal that the proposed ESMO-ResNet model on SARS-CoV-2 CT database achieves 91.23% accuracy, which is 21.46%, 20.2%, 12.4%, and 6% higher than the AlexNet, multi-source deep transfer learning (MSDTL), stacked convolutional neural network (S-CNN) and dynamic mutual training (DMT) models, respectively. Similarly, the ESMO-ResNet model on Covi-19 Radiography dataset achieves 90.06% accuracy, which is 21.34%, 20%, 9.7%, and 3.5% higher than AlexNet, MSDTL, S-CNN, and DMT models, respectively.

Keywords: COVID-19, Deep neural network, Spider monkey optimization, Discriminative features, Transfer learning.

1. Introduction

Coronavirus disease is the respiratory illness affected by severe acute repository syndrome (SARS-CoV-2)) which was detected in Wuhan, China in 2019. In short, this condition was known as Covid-19. As a result of the wide range of clinical signs and indications associated with COVID-19, the infection can transmit rapidly to other individuals through contact with them. These indications include fever, dyspnoea, drowsiness, myalgia and gastrointestinal issues [1]. Consequently, it is essential to detect and quarantine the afflicted individuals as soon as possible to prevent the virus from spreading.

Reverse transcription polymerase chain reaction (RT-PCR) is utilized to detect COVID-19 infection in RT-PCR technique, samples are collected in a body area where Covid-19 infections are frequently formed like the nose or throat. The sample is then chemically analysed for determining the coronavirus presences [2]. Although RT-PCR may provide distinguish result in detecting Covid-19 infections, this technology is not widely used in many regions of the world.

Consequently, CT scans and X-rays are used as a

suitable alternate method of detecting COVID-19. On the other hand, RT-PCR is expensive and takes a long time for the detection process. Clinical radiologists may experience difficulty in interpreting the results of various imaging procedure unexpectedly which results in lower accuracy and efficiency [3].

Machine learning (ML) techniques have been increasingly popular in recent years for medical imaging computer-aided detection. For instance, supervised ML algorithms with digital signal processing (MLDSP) was used [4] for COVID-19 identification using genomic fingerprints for identifying of new infections. In addition, a comprehensive analysis of various ML was published [5] for the instinctive Covid-19 identification from CXR using artificial neural network (ANN), support-vector machines (SVM), radial basis function (RBF), k-nearest neighbor (k-NN), decision tree (DT), and several designs of convolutional DL networks. In the initial period of the Covid-19 pandemic, an Ml algorithm [6] was constructed to forecast a confirmed SARS-CoV-2 contamination cases for RT-PCR examination by addressing the simple queries regarding SARS-CoV-2 symptoms to all the afflicted persons.

Although ML techniques increased Covid-19 virus detection accuracy, the training period is lengthy and inappropriate for large volumes of data. DL is a novel field that is critical in identifying several parts of the COVID-19 outbreak. This method enables immediate disease detection for analysing complex medical images [7]. According to the network structure, DL approaches are often classed as unsupervised pre-learned models, recurrent, recursive, and CNNs.

CNN is a popular DL method which aims to train clinical image structures and attributes for diagnosing all forms of disease using enhanced clinical images [8, 9]. In many cases, the experts utilize region-based CNNs to generate visual context, which aids in the identification of important results. There are several pre-trained CNN structures like VGGNet and ResNet are available to adopt the specific process in solving a problem by quickly learning the appropriate parameter.

To provide the effective detection of COVID-19 patients from and CT and CXR scanned images, a new TL-based uncertainty-aware technique [10] was developed. This method extracts important and distinctive features from and CT and CXR images in a systematic way using different qualitative CNN techniques using VGG16, DenseNet121, InceptinResNetV2, and ResNet50. ResNet50 provided better results for COVID-19 detection. However, this technique performed better only for selecting appropriate layer for ResNet architecture. An appropriate layers selected manually for given input image is highly challengeable.

This paper resolves the above-mentioned issues by utilizing ESMO algorithm for selecting appropriate layers of ResNet architecture. SMO algorithm [11] is a population-based algorithm that is mainly inspired by the social actions which are commonly performed by spider monkeys. The premature convergence rate SMO is improved in ESMO [12]. In ESMO, an improvised strategy is applied to update the position of solution towards local and global leader phase. The initialized group of SMs chooses a number of layer and a parameter to fine-tune the ResNet architecture. To find the best optimal solutions, the fitness (CCEL of ResNet for selected layers) of each SM is calculated. The position of each SM moves towards local and global leaders. The position update process repeated until all SMs have same fitness (CCEL). The feature extracted from ESMO-ResNet is trained and classified images as normal or COVID-19 using Softmax classifier.

The other sections of this paper are organized as follows: Section II reviews existing research works on detecting and diagnosing COVID-19 cases from XR and CT image datasets. Section III describes the functioning of the ESMO-ResNet technique and section IV illustrates its validity. Section V summarises the whole study and recommends potential possibilities.

2. Literature survey

A powerful CNN was developed [13] with a modified pre-learned AlexNet model to detect the COVID-19 pneumonia using CT and CXR images. This model makes advantage of an easily accessible CT scan and CXR images to make it more authentic in recognizing COVID-19 instances. The improved pre-trained DL model was then used to detect COVID-19 cases. However, this model requires additional features and large quantities of images to increase its accuracy.

A new method depending on the MSDTL was developed [14] to effectively monitor the prospective COVID-19 diseases. In this method, every province-related database was trained on a basic long short-term memory (LSTM) framework for forthcoming disease prediction in that domain. Also, the learned framework was fine-tuned by the MSDTL to achieve precise prediction. But, the accuracy was degraded while the gradient of disease range was low.

A novel S-CNN framework was developed [15] to automatically recognizing COVID-19 pulmonary disease from chest X-rays and CT scans. Various sub-

models were acquired from the VGG19 and the Xception frameworks during learning. Features from VGG19 Xception are combined by the softmax to categorize COVID-19 illness type. But, accuracy of this method is suffered for low contrast images.

A semi-supervised segmentation of COVID-19 infection was suggested [16] based on CT-scan lung using DMT. This model analyses the position and the region of the Covid-19 spread in the lungs using CT-scan images by segmentation. The DMT was utilized for the segmenting the lungs in areas affected with COVID-19. However, accuracy is affected, because of ambiguous boundaries in lung CT scans.

A metaheuristic method using tournament mechanism called quad tournament optimizer (QTO) was developed [17]. In QTO model, four searches like searching toward the global best solution, searching toward the middle between the global best solution and a randomly selected solution, searching relative to a randomly selected solution, and neighbourhood search around the corresponding solution and the global best solution were conducted by each agent in every iteration to find the best candidate. However, QTO was not tested to solve the practical optimization problem.

A new metaheuristic algorithm called multiple interaction optimizer (MIO) was developed [18] to solve the order allocation problem. MIO has distinct mechanics in finding the optimal solution. Initially, each agent interacts with some randomly selected agents in the population. The guided search was performed in every interaction. In the second phase, each agent carries out a local search which linearly reduces the search space during the iteration to solve the allocation issues.

A metaphor-free metaheuristic model called attack-leave optimizer (ALO) was developed [19]. ALO consists of four guided searches and one random search, performed in three phases in which two mandatory and one optional. In the first phase, the guided search is conducted with the best global solution as the reference. In the second phase, the guided search is conducted with a randomly selected solution as the reference. The random search is performed in the third phase. However, the looping process in the iteration phase affects the algorithms performances.

2.2 Research contribution

The main limitations noticed from the above literature work are the values of accuracy, precision, recall and F-measure are affected on various factors like uncertainty or missing data in the scanned images, finds difficulty in selecting proper learning parameters and low contrasted images. In contrast with the literature works, a new DL classifier is developed in this paper with optimizing the layers of DL classifier for achieving high accuracy.

Table 1. Notation list

SM_a	a^{th} SM in the swarm
SM_p	Population's p^{th}monkey
M	Maximum number of variables
SM_{max_b} & SM_{min_b}	Upper and Lower bounds of the search space in b^{th} dimension, Where $b = 1,2..M$.
SM_{ab}	b^{th} dimension of the a^{th} SM
GL_b	The GL location in b^{th} dimension
fn	SM's fitness
fn_a	a^{th} SM's fitness value
$\phi_{a,b}$ is a	Consistently determined arbitrary number in the interval [0,1]
ESM_{ab}	b^{th} dimension of the a^{th} ESM
a	Sample images from a total of K sample images, ,
b	from a total set of c classes
x	represents the sample label
$prob_a$	Selection probability

3. Proposed methodology

The developed method for Covid-19 detection utilizing ESMO-ResNet is briefly presented in this section. The schematic illustration of the proposed structure for Covid-19 diagnostics and detection is shown in Fig. 1. The Table 1 depicts the notation list of this framework.

3.1 TL with fine tuning process

Training CNN from scratch (arbitrary configuration) often necessitates a large number of labelled training examples that must be evaluated with more processing capability, resulting in a less time-consuming effort. In such cases, employing TL techniques could provide significant benefits in terms of both time complexity and the larger datasets complications. In general, the transfers learning are processed in different pathways like fine-tuning and freezing. The weights and biases of a pre-trained ResNet are employed for fine-tuning followed by a normal training approach on the target dataset.

Pre-learned ResNet levels function as a constant feature extractor in the freezing configuration, while the other retrieved attributes are sent into the classifier. In this example, the convolutional layers' weights and biases are locked, but the highly connected layers are fine-tuned over the intended dataset. The proposed work will focus on the first

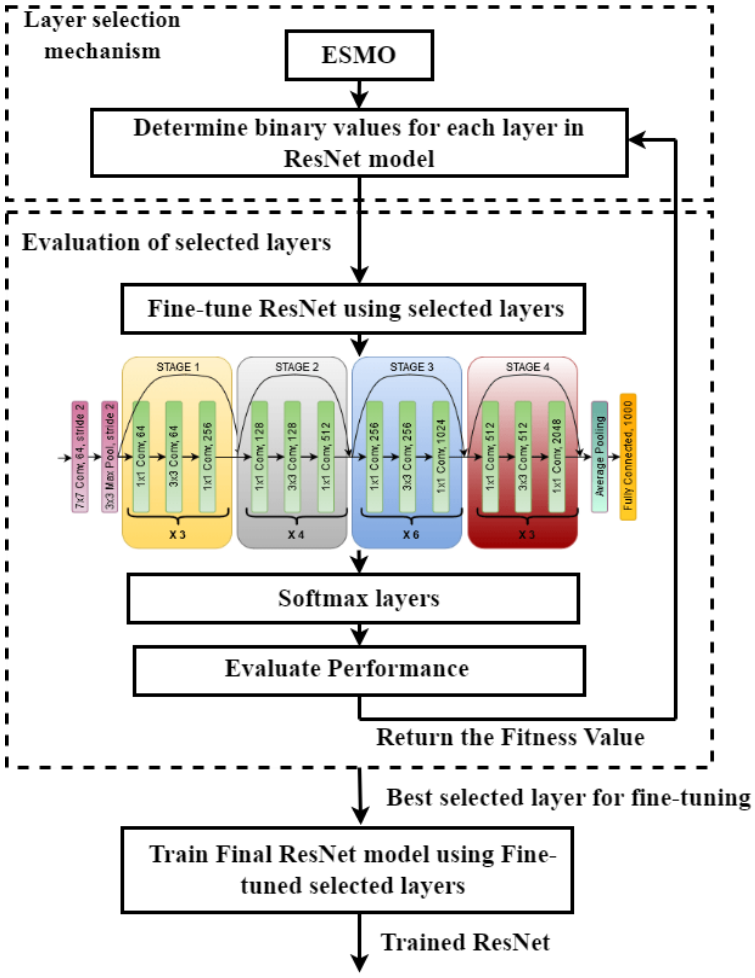

Figure. 1 Schematic structure of proposed model

scenario in which the TL technique will be used as the fine-tuning mechanism due to the huge disparity between the source and targeted image datasets. Fine-Tuning process in TL steps ate

Step 1: Pre-training the neural network model (target model) using the source dataset (e.g., the ImageNet dataset).

Step 2: Construct a neural network model (target model) which duplicates all the input parameters and features from the targeted model apart for the output layer. Consider these system variables represent an information gained from the original dataset, and this knowledge will be also relevant to the destination dataset. Also, presume the source model's output layer which is strongly tied to the source labels dataset and thus, it will not be used in target model.

Step 3: Insert an output layer to the objective network with the same number of outputs as the target dataset's categories. Then, arbitrarily set the model parameters for this layer.

Step 4: The target model is trained using the source dataset. The output layer will be generated from scratch, while the remaining layers' parameters will be effectively validated using the original network parameters.

When the targeted datasets are significantly shorter than the original datasets, the calibration approach will help to improve model's generalization.

3.2 SMO algorithm

SMO is a heuristic-enhanced approach [11] inspired by the adaptive searching behaviour of SMs. A fission-binding social architecture underlies With SM foraging behaviour. In the social organization of the specific group, a female leader will decide either to separate or to integrate based on the qualities of this algorithm. The global leader (GL) leads the main category, while the local leaders (L^2) dominate the subsidiary category. Based to the SMO algorithm, food scarcity is indicated by a lack of progress in solution. Because SMO is built on swarm intelligence, each smaller component must have a different number of monkeys.

For the proposed work, SMO is divided into six phases: the local leader phase (L^2 P), the GL phase (GLP), L^2 learning phase (L^3), the GL learning phase (GL^2P), the L^2 decision phase (L^2 DP), and the GL

decision phase (GLDP). All of these stages of SMO are depicted briefly here.

3.2.1. Initializing the population

SMO allocates the population A in SM, consistently which is defined as SM_a, where $a = 1,2 \ldots A$. Monkeys are M-dimensional vectors with higher number of variables in the challenge domains. Each SM_a corresponds to a single alternative response to the specified problem. SMO uses the preceding equation to initialise each SM_a in Eq. (1),

$$SM_{ab} = SM_{min_b} + R(0,1) \times (SM_{max_b} - SM_{min_b}) \quad (1)$$

Where, R (0,1) is an arbitrary integer generated consistently throughout the range from 0 to 1.

3.2.2. Local leader phase (L^2P)

This is a critical stage in the SMO. In L^2P, the SM adjusts its present position by depending upon both L^2 and their local group members (LGM). The SM's location is modified only when the new place has a greater fitness level than the prior location. The following is the equation for updating the location of the a^{th} SM of the p^{th} local category as given in Eq. (2),

$$SM_{new_{ab}} = SM_{ab} + R(0,1) \times \left(LL_{pb} - SM_{ab}\right) + R(-1,1) \times (SM_{tb} - SM_{ab}) \quad (2)$$

Where LL_{pb} represents the b^{th} dimensions of the p^{th} LGP position. SM_{tb} signifies the b^{th} dimension of the arbitrarily selected p^{th} SM local group, where $r \neq a$ is a consistently dispersed arbitrary integer ranging from −1 to 1.

3.2.3. Global leader phase (GLP)

In GLP, experiences of GL and LGM are used to upgrade the position of all the SM. The position updated equation is given as Eq. (3)

$$SM_{new_{ab}} = SM_{ab} + R(0,1) \times \left(GL_{pb} - SM_{ab}\right) + R(-1,1) \times (SM_{tb} - SM_{ab}) \quad (3)$$

The SM fitness fn is used in this step to determine probability $prob_a$. SM_a position is modified based on the possibility integer. Candidates with better locations will enhance the number of possibilities in GL. The following is the probability evaluation in Eq. (4)

$$prob_a = \frac{fn_a}{\sum_{a=1}^{N} fn_a} \quad (4)$$

Furthermore, the appropriateness of the SM's new site is evaluated and distinguished from that of the previous place. The position with the maximum fitness value will be deliberately selected.

3.2.4. Global leader learning (GLL) phase

A greedy selection strategy is used to modify the GL position. The GL position will be adjusted with the position of the SM with the highest fitness score in the population. The best position is chosen for the GL. If no further changes are found, the global limitation number is increased by one.

3.2.5. Local leader learning phase (L^3P)

A greedy selection method (GSM) is used in the LGM to upgrade the L^2 position. The position of the L^2 is modified with the SM location to achieve the highest fitness in a specific local group. The L^2 is granted with an optimum location. If no more upgrades are detected, a 1 is added to the local limit count.

3.2.6. Local leader decision (L^2D) phase

When a L^2 fails to upgrade its position within a defined L^2 Limit, all members in that local group adjust their positions in a constant way, as described in step 1, or by leveraging previous knowledge from the GL and L^2, as described in Eq. (5)

$$SM_{new_{ab}} = SM_{ab} + R(0,1) \times \left(GL_{pb} - SM_{ab}\right) + R(0,1) \times (SM_{tb} - LL_{ab}) \quad (5)$$

3.2.7. Global leader decision (GLD) phase

When a GL fails to modify its position up to the global leader limit, the population divides into minor groups based on the GL's decision. This group splitting process is repeated until the optimum range of groups (MG) is reached. A L^2 is chosen for the newly formed group at each iteration. If the GL creates the highest range of permissible groups and does not upgrade its location until the predetermined permitted restriction is reached, the GL determines to combine the whole category into a single category. The following parameters govern SMO processing:

- Importance of local leader limit
- Global leader limit
- Max number of group (MG)
- Perturbation range (Pr)

3.2.8. Enhanced SMO (ESMO)

The ESMO [12] improves on the basic SMO algorithm's performance. The ESMO recommended various changes to the L^2P of basic SMO. ESMO's position update equation takes the average of the difference between the current position and randomly generated positions. For a given problem, it generates a random place within a certain range. This suggested change speeds up the convergence rate and increases reliability. It is expected that the better suited solution has an optimal solution in their proximity.

$$SM_{new_{ab}} = SM_{ab} + \phi_{a,b}\left(L^2_{sb} - ESM_{ab}\right) + \phi_{a,b}\frac{Sum}{SN} \quad (6)$$

In Eq. (6), L^2_{sb} guarantees the dimension of the L^2 group posistion. The SN represents the food source's position, which is generated at random. $Sum = Sum + (SM_{ab} - L^2_{sb})$, where Sum is the average of the difference between the present position and the randomly generated position. This equation improves highly fitted answers by drawing on the best swarm intelligence. This ESMO improves the balance between exploring and exploiting the most viable ideas.

3.3 Adaptive fine-tuning with ESMO algorithm

The adaptive ESMO technique was created to optimise the layers of CNN (ResNet) architecture. The ESMO method is employed in this procedure to identify the most efficient solution to the issue of locating and identifying the CNN tiers for adjustments, which may instantly be changed into an optimizing problem. In order to produce the best CNN, the response will be an appropriate layer decision that needs be examined for fine-tuning.

The ESMO-Fine tuning approach is composed of two systems like layer selection and layer evaluation. The layer selection approach is responsible for providing independent values, i.e., a range of discrete integers, where every number in the array indicates whether or not the appropriate layer of the CNN framework is considered for fine-tuning. The assessment component fine-tunes and analyses the anticipated efficiency of the CNN network depending on the supplied individual. CNN is evaluated using a fitness function, particularly by using well-known function called categorical cross- entropy loss (CCEL).

The fitness value is passed back to the layers selection process, which creates a distinct individual based on the performance of assessment score. The process is repeated until the optimum range of sample evaluations is reached, with the purpose of reducing the fitness value to the minimum. The maximum range of model evaluations represents the maximum number of individuals developed by the ESMO sequence, which is a completely modifiable variable. The following subsections go over every of the ESMO - Fine tuning procedures in depth.

3.3.1. Mechanism for layer selection

The layer selection technique will be based on the ESMO algorithm, which has been updated to decide fine-tuned CNN layers, some of which will be frozen. It is absolutely important to update the characterization of individuals in order to perform layer selection using the ESMO method.

Individuals in the developed ESMO- Fine tuning technique will be represented as an vector with actual integers which can be significantly defined as shown in Eq. (7), for $a = 0, \dots, n_s$, in which every layer $X^{(u)}_{a,0}$ for $a = 0, \dots, n$ is selected from the particular range [0, 1], T is the threshold integer utilized for mapping operations and n represents the complete layers presented in the selected CNN structure.

$$X^{(u)}_a = \left(X^{(u)}_{a,0}, .., X^{(u)}_{a,n}, tv^{(u)}_a\right), \quad (7)$$

The shifting criterion is used to acquire more varied individuals. The moving threshold approach works by including the threshold number for every individual response vector, which is then constantly adjusted for each solution candidate, reducing the requirement for periodic adjustment. Furthermore, this procedure may result in more potentially varied individuals. Eq. (8) establishes whether or not the associated layer is accessible for fine-tuning depending upon the T values.

$$v^{(u)}_{a,b} = \begin{cases} 1, \ if X^{(u)}_{a,0} > T^u \\ 0, \ Otherwise \end{cases} \quad (8)$$

The particular vector v_a represents the mapped sequence of binary numbers ($0\ and\ 1$) for the a^{th}participant, where the number 0 for the b^{th}layer indicates a layer that is not recognized for fine tuning and the number 1 denotes a layer that is selected for fine tuning.

3.3.2. Analysis of selected layers

CNN is fine-tuned for every individual v - generated as explained in the prior subsection. A fitness function F is devised to evaluate how good or poor the created individual is. Following the fine-

tuning of the CNN layers based on the supplied person, the fitness function is constructed and passed to the ESMO algorithm, allowing the ESMO to search for best participant. The fine-tuning is carried out for a set number of periods, after which the earlier termination approach is used to end the fine-tuning of unwanted layer configurations. The optimum range of epochs is a completely personalised variable that should be adjusted in accordance to the desired datasets. A CCEL score is used to assess the effectiveness of a suggested model that has been learned by fine-tuning the layers which is chosen by the generated individual. It is formally expressed as in Eq. (9),

$$F = CCEL = -\frac{1}{K}\sum_{i=1}^{K}\sum_{j=1}^{c} x_{a,b}\log(s_{ij}) \quad (9)$$

$Where, s_{ij} \in (0,1) : \sum_b s_{ij} = 1 \forall a, b$ denotes a sample prediction.

3.4 Training the final CNN model

In order to achieve the performance of classifier due to optimal layer selection, a subset of 80% of the training instance should be selected during the ESMO procedure for training CNN structure depending on the ESMO algorithm's particular possibility. Eq. (7) will be used to evaluate the qualified CNN structure performance with the residual 20% of the testing set. The optimal functioning method is determined after viewing all conceivable options, and the fine-tuning layer integration is used to fine-tune the final CNN layers. Unlike models generated on candidate solutions, this whole ResNet structure is constructed from the beginning on the complete training data. The developed ESMO-fine tune approach will produce the final CNN network.

ESMO Algorithm for selecting ResNet layers
Input: Initialized Number of ResNet layers
Output: Selected Layer
Step 1; Utilize EMSO model for selecting the ResNet layer
Initialize the population (layers), L^2 limit, GL limit, and P_r by using the Eq. (1)
Identify L^2 and GL;
Position update by L^2P and GLP depending upon the LGM (as per the Eq. (6) & (3));
Compute the probability $prob_i$ for each candidate of the category using Eq. (4)
Training the layers through L^3P and GLL phase
If L^2P is not updating their position after a specified number of iterations, then redirect the L^2P as per the Eq. (5)
If GLP is not updating their position after a specified number of iterations, then divide the groups into smaller groups.
Step 2: After the selection process, fine-tune the selected ResNet layers using Eq. (8)
Step 3: Calculate the fitness function using Eq. (9)
Step 4: If fitness function is satisfied, train the final ResNet using best (fine-tuned) selected layers, or else return to step 1.

4. Dataset description

For the experimental analysis, the datasets are collected from different websites which are listed below.

4.1 SARS-CoV-2 CT database

SARS-CoV-2 CT dataset is collected from [20] which consists of 1252 Covid-19 positive images and 1230 Covid-19 negative images, totally 2482 CT images. For the experimental purpose, 60% (751 images form Covid-19 positive images and 738 images from Covid-19 negative images) are used for training and the remaining 40% (500 images form Covid-19 positive images and 492 images from Covid-19 negative images) are used for testing. The Normal and COVID-19 images from CT scans is depicted in Fig. 2.

4.2 Covid-19 radiography database

Database of Covid-19 Radiography is collected from [21]. The first version of dataset consists of 219 COVID-19 and 1341 normal images. The second versions of dataset consists of 3616 COVID-19 and 10,192 normal images. Totally 3835 COVID-19 images and 11533 normal images available in the dataset. Since, the balanced images for both classes required for training and testing, totally, 3835 COVID-19 and 3835 normal images are considered for experiments. For the training, 60% (2301 images form Covid-19 cases and 2301 from normal cases) of images are used. For testing, 40% (1534 images form Covid-19 cases and 1534 from normal cases) of images are used. Fig. 3 depicts the normal and COVID-19 images from CXR image dataset.

5. Result and discussion

The performance of ESMO-ResNet and existing classification algorithms like AlexNet [13], MSDTL [14], S-CNN [15] and DMT [16] are implemented in MATLAB 2017b for SARS-CoV-2 CT and CXR dataset. The below Tables 1 and 2 provides the confusion matrix for CT images and CXR images

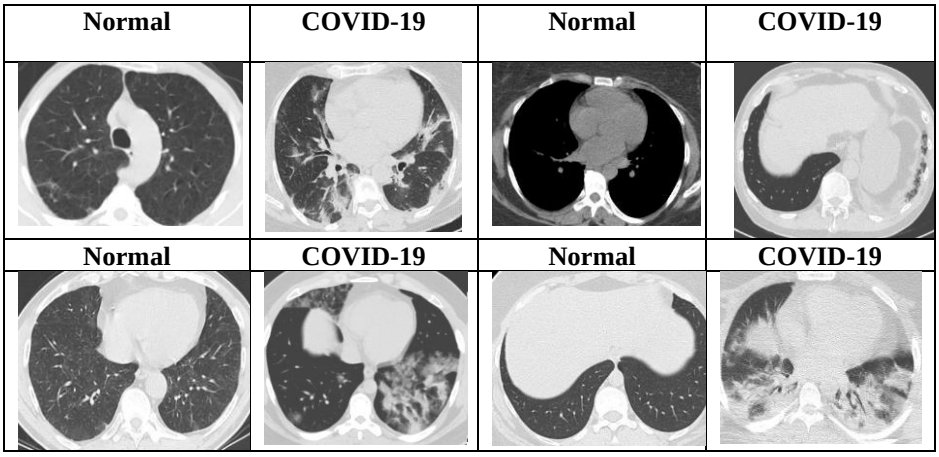

Figure. 2 CT images for normal and Covid-19 cases

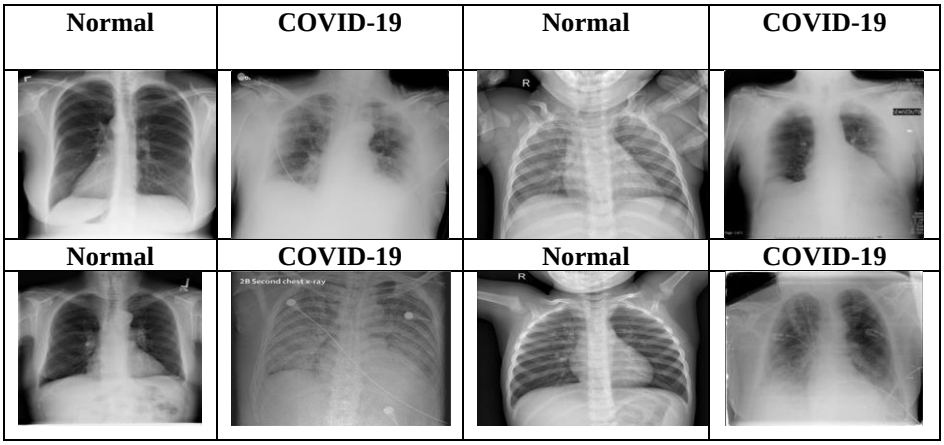

Figure. 3 CXR images for normal and Covid-19 case

Table 1. Confusion matrix for SARS-CoV-2 CT database

SARS-CoV-2 CT Database				
Methods	**TP**	**TN**	**FP**	**FN**
AlexNet	375	370	123	124
MSDTL	381	372	119	120
S-CNN	406	399	93	94
DMT	430	424	68	70
ESMO-ResNet	457	448	43	44

Table 2. Confusion matrix for Covid-19 radiography database

Covid-19 Radiography Images				
Methods	**TP**	**TN**	**FP**	**FN**
AlexNet	1138	1139	395	396
MSDTL	1151	1152	382	383
S-CNN	1257	1261	274	276
DMT	1336	1334	200	198
ESMO-ResNet	1382	1381	153	152

respectively.

True positive (TP) and true negative (TN) solutions are those in which the classifier predicts the covid-19 and normal situations as themselves, respectively. False positive (FP) solutions occur when the classifier incorrectly identifies a normal case as Covid-19 instances, whereas false negative (FN) responses occur when the classifier incorrectly predicts the Covid-19 as normal. Based on the above confusion matrix, the efficiency of the proposed method is evaluated using different evaluation metrics which are described below.

5.1 Accuracy

Accuracy is an essential parameter for assessing classification systems, and it is characterized as the ratio of accurate COVID-19 forecasts to entire observations conducted by using the provided data sample. The accuracy percentage can be estimated as in Eq. (10),

$$Accuracy = \frac{TP+TN}{TP+TN+FP+FN} \quad (10)$$

Fig. 4 demonstrates the accuracy values obtained by MSDTL, S-CNN and DMT and ESMO-ResNet models for Covid-19 identification using SARS-CoV-2 CT scan dataset and Covid-19 radiography

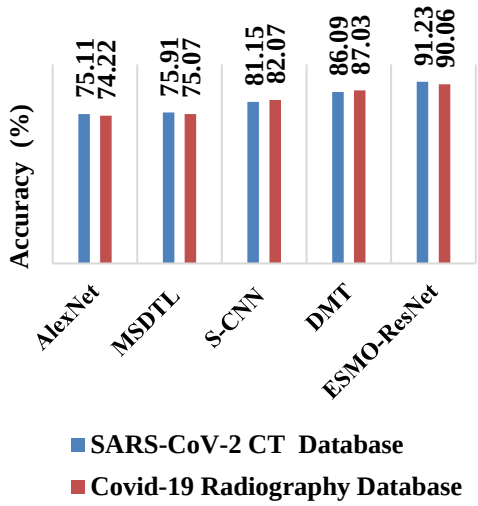

Figure. 4 Comparison of accuracy

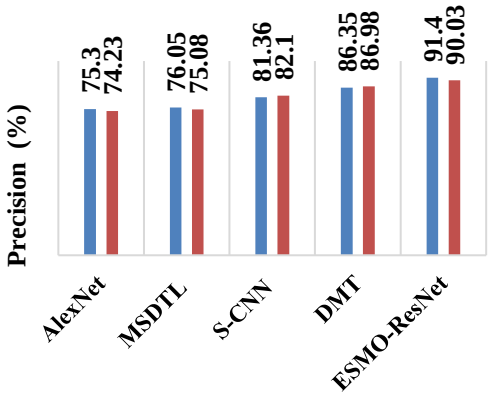

Figure. 5 Comparison of precision

dataset. This analysis shows that the proposed ESMO-ResNet model outperforms the AlexNet, MSDTL, S-CNN, and DMT models in terms of accuracy, with the accuracy of the ESMO-ResNet model being 21.46% and 21.34% higher than AlexNet, 19.94% and 19.98% higher than MSDTL, 12.19%, and 9.74% higher than S-CNN, and 5.76% and 3.48% higher than the DMT models for SARS-CoV-2 CT and Covid-19 radiography database.

5.2 Precision

It is the ratio of exactly classified categories of Covid-19 cases at TP and FP rates.

$$Precision = \frac{TP}{TP+FP} \tag{11}$$

Fig. 5 demonstrates the precision values obtained by MSDTL, S-CNN and DMT and ESMO-ResNet models for predicting the Covid-19 cases using

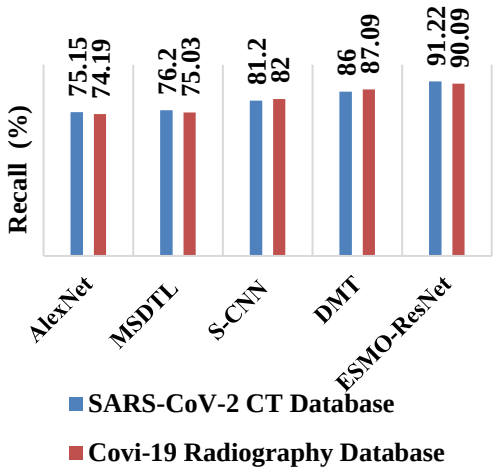

Figure. 6 Comparison of recall

SARS-CoV-2 CT scan dataset and Covid-19 Radiography dataset. By using this analysis, it is obtained that the proposed SMO-CNN achieves a higher precision compared to the AlexNet, MSDTL, S-CNN and DMT models i.e., the precision of ESMO-ResNet model is 21.38% and 21.29% higher than AlexNet, 19.91% and 19.48% higher than MSDTL, 12.12% and 9.67% higher than S-CNN, 5.63% and 3.50% higher than the DMT models for SARS-CoV-2 CT and Covid-19 radiography database.

5.3 Recall

It is the ratio of exactly classified categories of Covid-19 cases at TP and FN rates.

$$Recall = \frac{TP}{TP + FN} \tag{12}$$

Fig. 6 demonstrates the recall values obtained by MSDTL, S-CNN and DMT and ESMO-ResNet models for identifying the Covid-19 cases using SARS-CoV-2 dataset and Covid-19 Radiography dataset. This analysis shows that the proposed ESMO-ResNet model outperforms the AlexNet, MSDTL, S-CNN and DMT and ESMO-ResNet in terms of recall, with the recall of the ESMO-ResNet model being 21.39% and 21.43% higher than AlexNet, 19.47% and 20.07% higher than MSDTL, 12.12% and 9.75% higher than S-CNN, and 5.86% and 3.44% higher than the DMT models for SARS-CoV-2 CT and Covid-19 radiography database, respectively.

5.4 F-measure

It is defined as the weighted average of precision and recall, with a value of '1' being the highest and a value of '0' representing the lowest.

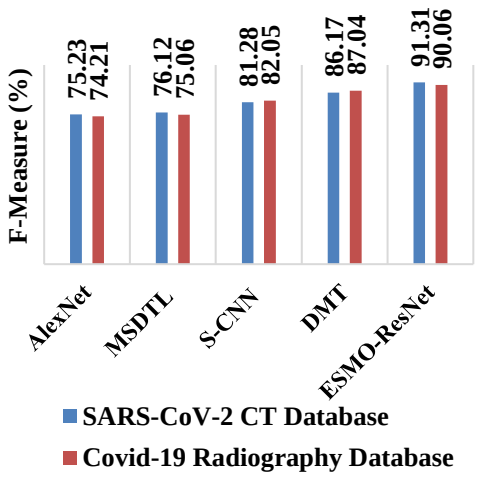

Figure. 7 Comparison of F-measure

$$F-measure = 2 \times \frac{Precision \cdot Recall}{Precision+Recall} \quad (13)$$

The F-measure values produced by the MSDTL, S-CNN and DMT and ESMO-ResNet structures for Covid-19 identification utilising SARS-CoV-2 CT scan dataset and Covid-19 Radiography dataset are shown in Fig. 7. By using this analysis, it is obtained that the proposed ESMO-ResNet achieves a higher F1-Score compared to the AlexNet, MSDTL, S-CNN and DMT models i.e., the F1-Score of ESMO-ResNet model is 21.37% and 29.44% higher than AlexNet, 19.98% and 19.98% higher than MSDTL, 12.36% and 9.71% higher than S-CNN, 5.98% and 3.46% higher than the DMT models for SARS-CoV-2 CT and Covid-19 Radiography Database respectively.

6. Conclusion

This paper proposed ESMO-ResNet for identifying Covid-19 instances from CT and CXR images. The ESMO fine-tuned layers of ResNet architecture in order to reduce the classification error for given input image. The procedure takes on the issue of deciding which of a set of provided layers to fine-tune and which to abandon frozen, for the most accurate classification performance. A fine-tuned layer selection automatically improve the performance measure of Covid-19 detection. Finally, the results reveal that the proposed ESMO-ResNet model on the SARS-CoV-2 CT database achieves 91.23% accuracy, whereas the accuracy of AlexNet, MSDTL, S-CNN, and DMT models is 75.11%, 75.91%, 81.15%, and 86.09%, respectively. Similarly, the ESMO-ResNet model on Covid-19 Radiography Database achieves 90.06% accuracy while the AlexNet, MSDTL, S-CNN, and DMT models achieve 74.22%, 75.07%, 82.07%, and 87.03% accuracy, respectively. More comprehensive estimation of the uncertainty measures will be investigated based on heretical feature learning to improve prediction in future.

Conflict of interest

The authors declare no conflict of interest.

Author contributions

Conceptualization, methodology, software, validation, Deepika; formal analysis, investigation, Rajeshwari; resources, data curation, writing—original draft preparation, Deepika; writing—review and editing, Deepika; visualization, supervision, Rajeshwari.

References

[1] S. G. Fard, R. Noroozi, R. Vafaee, W. Branicki, E. Pośpiech, K. Pyrc, and M. Sanak, “Effects of host genetic variations on response to, susceptibility and severity of respiratory infections”, *Biomedicine & Pharmacotherapy*, Vol. 128, pp. 110296, 2020.

[2] I. Smyrlaki, M. Ekman, A. Lentini, N. R. D. Sousa, N. Papanicolaou, M. Vondracek, and B. Reinius, “Massive and rapid COVID-19 testing is feasible by extraction-free SARS-CoV-2 RT-PCR”, *Nature Communications*, Vol. 11, No. 1, pp. 1-12, 2020.

[3] H. X. Bai, B. Hsieh, Z. Xiong, K. Halsey, J. W. Choi, and T. M. L. Tran, “Performance of radiologists in differentiating COVID-19 from viral pneumonia on chest CT”, *Radiology*. Vol. 296, pp. 1–8, 2020.

[4] G. S. Randhawa, M. P. Soltysiak, H. E. Roz, C. P. D. Souza, K. A. Hill, and L. Kari, “Machine learning using intrinsic genomic signatures for rapid classification of novel pathogens: COVID-19 case study”, *Plos one*, Vol. 15, No. 4, pp. e0232391, 2020.

[5] M. Abed, K. H. Mohammed, G. Z. Abdulkareem, M. Begonya, A. Salama, M. S. Maashi, and L. Mutlag, “A comprehensive investigation of machine learning feature extraction and classification methods for automated diagnosis of COVID-19 based on X-ray images”, *Computers, Materials, & Continua*, Vol. 66, No. 3, pp. 3289-3310, 2021.

[6] Y. Zoabi, S. D. Rozov, and N. Shomron, “Machine learning-based prediction of COVID-19 diagnosis based on symptoms”, *Npj Digital Medicine*, Vol. 4, No. 1, pp. 1-5, 2021.

[7] S. Bhattacharya, P. K. R. Maddikunta, Q. V. Pham, T. R. Gadekallu, C. L. Chowdhary, M.

Alazab, and M. J. Piran, "Deep learning and medical image processing for coronavirus (COVID-19) pandemic: A survey", *Sustainable Cities and Society*, Vol. 65, p. 102589, 2021.

[8] L. Li, L. Qin, Z. Xu, Y. Yin, X. Wang, B. Kong, and J. Xia, "Artificial intelligence distinguishes COVID-19 from community acquired pneumonia on chest CT", *Radiology*, 2020.

[9] K. Jaiswal, P. Tiwari, S. Kumar, D. Gupta, A. Khanna, and J. J. Rodrigues, "Identifying pneumonia in chest X-rays: a deep learning approach", *Measurement*, Vol. 145, pp. 511-518, 2019.

[10] A. Shamsi, H. Asgharnezhad, S. S. Jokandan, A. Khosravi, P. M. Kebria, D. Nahavandi, S. Nahavandi, and D. Srinivasan, "An Uncertainty-Aware Transfer Learning-Based Framework for COVID-19 Diagnosis", *IEEE Transactions on Neural Networks and Learning Systems*, Vol. 32, No, 4, pp. 1408-1417, 2021.

[11] H. Sharma, G. Hazrati, and J. C. Bansal, "Spider monkey optimization algorithm", *Evolutionary and Swarm Intelligence Algorithms*, pp. 43-59, 2019.

[12] P. R. Singh, D. Moussa, X. Shengwu, and B. P. Singh, "Improved Spider Monkey Optimization Algorithm to train MLP for data classification", *3c Tecnología: Glosas De Innovación Aplicadas A La Pyme*, Vol. 8, No. 1, pp. 142-165, 2019.

[13] S. Wang, B. Kang, J. Ma, X. Zeng, M. Xiao, J. Guo, and B. Xu, "A deep learning algorithm using CT images to screen for corona virus disease (COVID-19)", *European Radiology*, Vol. 14, pp. 1-9, 2021.

[14] S. Garg, S. Kumar, and P. K. Muhuri, "A novel approach for COVID-19 Infection forecasting based on Multi-Source Deep Transfer Learning", *Computers in Biology and Medicine*, Vol. 149, pp. 1-16, 2022.

[15] M. Gour and S. Jain, "Automated COVID-19 detection from X-ray and CT images with stacked ensemble convolutional neural network", B*iocybernetics and Biomedical Engineering*, Vol. 42, No. 1, pp. 27-41, 2022.

[16] E. Resita, T. Karlita, R. Sigit, E. M. Yuniarno, I. K. E. Purnama, and M. H. Purnomo, "Semi-Supervised Segmentation of COVID-19 Infection on CT-Scan Lung Using Dynamic Mutual Training", *International Journal of Intelligent Engineering and Systems*, Vol. 15, No. 5, 2022, doi: 10.22266/ijies2022.1031.47.

[17] P. D. Kusuma and M. Kallista, "Quad Tournament Optimizer: A Novel Metaheuristic Based on Tournament among Four Strategies", *International Journal of Intelligent Engineering & Systems*, Vol. 16, No. 2, 2023, doi: 10.22266/ijies2023.0430.22.

[18] P. D. Kusuma and A. Novianty, "Multiple Interaction Optimizer: A Novel Metaheuristic and Its Application to Solve Order Allocation Problem", *International Journal of Intelligent Engineering & Systems*, Vol. 16, No. 2, 2023, doi: 10.22266/ijies2023.0430.35.

[19] P. D. Kusuma and F. C. Hasibuan, "Attack-Leave Optimizer: A New Metaheuristic that Focuses on The Guided Search and Performs Random Search as Alternative", *International Journal of Intelligent Engineering & Systems*, Vol. 16, No. 3, 2023, doi: 10.22266/ijies2023.0630.19.

[20] https://www.kaggle.com/plameneduardo/sarscov2-ctscan-datase.

[21] https://www.kaggle.com/datasets/tawsifurrahman/covid19-radiography-database